

1  
2 **Dependence of precipitation on precipitable water vapor over the Maritime**  
3 **Continent and implications to the Madden-Julian Oscillation**  
4

5 **Siyue Chen<sup>1,2</sup>, Nathanael Z. Wong<sup>2</sup>, Ding Ma<sup>2</sup>, Pak Wah Chan<sup>2</sup>†, Zhiming Kuang<sup>2,3</sup>**

6 <sup>1</sup>Department of Atmospheric and Oceanic Sciences, School of Physics, Peking University,  
7 Beijing, China.

8 <sup>2</sup>Department of Earth and Planetary Sciences, Harvard University, Cambridge, MA, USA.

9 <sup>3</sup>John A. Paulson School of Engineering and Applied Sciences, Harvard University, Cambridge,  
10 MA, USA.

11 †Now at College of Engineering, Mathematics and Physical Sciences, University of Exeter,  
12 Exeter, UK.

13  
14 Corresponding author: Siyue Chen ([siyue\\_chen@fas.harvard.edu](mailto:siyue_chen@fas.harvard.edu))  
15  
16

17 **Key Points:**

- 18 • The dependence of precipitation on precipitable water vapor is stronger over ocean than  
19 over the Maritime Continent.  
20 • The MJO modulates the precipitable water vapor over the ocean and over the Maritime  
21 Continent by roughly the same amount.  
22 • Weaker precipitation variations over the Maritime Continent between the MJO phases  
23 may be explained by the weaker water vapor dependence.  
24

**25 Abstract**

26 The weakening of the Madden-Julian Oscillation (MJO) as it propagates over the Maritime  
27 Continent (MC) is often referred to as the MC barrier. Here, we use 3-hourly precipitable water  
28 vapor (PWV) data obtained from the Sumatran GPS Array and the ERA5 reanalysis to  
29 investigate the role played by the column moisture over the MC. Over Sumatra and the whole  
30 MC, we find a stronger dependence of precipitation on PWV over the ocean as compared to both  
31 inland and coastal regions. The MJO modulates the PWV over the ocean and over the MC by  
32 roughly the same amount, and the weaker precipitation variations over the MC between the MJO  
33 phases may be interpreted in terms of its weaker dependence on PWV over the MC. This  
34 different precipitation dependence on column moisture between the MC and the ocean may  
35 contribute to the MC barrier effect.

**36 Plain Language Summary**

37 The Madden-Julian Oscillation (MJO) is the dominant intraseasonal variability in the tropical  
38 atmosphere, and also influences the global climate and weather, including the El Niño-Southern  
39 Oscillation and the North Atlantic Oscillation. However, the reason behind why the MJO  
40 weakens or terminates as it propagates over the Maritime Continent remains unclear. Based on  
41 the idea that the rainfall is highly sensitive to the water vapor in the troposphere, we examine  
42 observations and reanalysis data. We find a weaker dependence of rainfall on column water  
43 vapor over the Maritime Continent than over the oceans, which may provide a simple  
44 interpretation of the smaller changes of rainfall over land associated with the MJO.

**45 1 Introduction**

46 The Madden-Julian Oscillation (MJO) is the dominant component of the intraseasonal  
47 (30-90 days) variability in the tropical atmosphere (Madden & Julian, 1971, 1972). In a typical  
48 MJO event, a convectively active envelope of precipitation develops over the western Indian  
49 Ocean and slowly propagates eastward along equator to the Pacific Ocean. Over the past  
50 decades, there have been extensive studies into both the mechanisms of the MJO and its  
51 interaction with the extratropical weather, and other large-scale modes of variability [e.g. the  
52 Asian monsoon, the El Niño-Southern Oscillation (ENSO), the North Atlantic Oscillation  
53 (NAO), etc.] (e.g. Kiladis & Weickmann, 1992; Mo, 2000; Zhang, 2005; Schreck et al., 2013;  
54 Zhou et al., 2016; Tippett, 2018; Barrett, 2019; Arcodia et al., 2020).

55 The Maritime Continent (MC) is a region in the tropics dominated by islands, many of  
56 which fall along the path of the MJO (Yamanaka, 2016). The MJO acts to modulate the rainfall  
57 and local land-sea circulation over the MC (Tian et al., 2006; Fujita et al., 2011). Recent  
58 observational analysis shows that the MC appears to be a barrier to the MJO propagation – some  
59 MJO events become weaker over the MC as they propagate into Pacific Ocean, while some  
60 terminate over the MC (Rui & Wang, 1990; Zhang & Ling, 2017). Model simulations show  
61 relatively low skills in representing this barrier effect (Inness et al., 2003; Seo et al., 2009; Vitart  
62 & Molteni, 2010; Weaver et al., 2011; Wang et al., 2019). Rainfall variance associated with the  
63 MJO is also markedly lower over the islands compared to their surrounding oceans (Maloney &  
64 Sobel, 2004).

65 Previously proposed mechanisms for this barrier effect involve, for example, local  
66 orography and the strong diurnal cycle over land. Maloney & Sobel (2004) attributed the smaller  
67 MJO modulation of the rainfall over the islands to the fact that land surfaces have lower sensible

68 and latent heat capacity compared to the ocean. Inness & Slingo (2006) and Wu & Hsu (2009)  
69 suggested that the elevated orography over the islands could act to block the propagation of low-  
70 level pressure and wind signal, which may disrupt the MJO propagation. Previous studies have  
71 also attributed the weakening of the MJO over the MC to the strong diurnal cycle over land and  
72 related phenomena (Neale & Slingo, 2003; Rauniyar & Walsh, 2011; Hagos et al., 2016; Majda  
73 & Yang, 2016). For example, the strong diurnal cycle of convection over islands increases the  
74 cloud cover and decreases surface insolation, which results in the lower precipitation rate over  
75 land in the MC (Rauniyar & Walsh, 2011). After removing the diurnal cycle of the incoming  
76 shortwave radiation at the top of the atmosphere, it was found through numerical simulations of a  
77 MJO event that the MJO could propagate more smoothly through the MC (Hagos et al., 2016).

78 Our work is motivated by the possibility of interpreting this barrier effect of the MC in  
79 the “moisture mode” framework for the MJO (e.g. Raymond, 2001; Andersen & Kuang, 2012;  
80 Sobel & Maloney, 2012, 2013; Adames & Kim, 2016). Recognizing the long timescale  
81 associated with the MJO compared to that of convectively coupled equatorial waves, the  
82 moisture mode framework of the MJO takes the column integrated moisture, instead of  
83 temperature or buoyancy, as the central component, and focuses on the processes that modify the  
84 column integrated moisture when considering the generation and propagation of the MJO. In  
85 terms of the generation, the moisture mode framework postulates that the MJO arises from a  
86 positive feedback in which an anomalously moist atmospheric column precipitates more, and the  
87 combined effect of anomalous radiative and surface fluxes and anomalous advection due to the  
88 resulting circulation further leads to an even moister column, resulting in a positive feedback  
89 loop. For a recent review on the moisture mode framework, see Adames & Maloney (2021).

90 In our paper, we emphasize the first half of the aforementioned feedback loop, namely  
91 that an anomalously moist atmospheric column precipitates more. Based on the daily rainfall and  
92 PWV derived from microwave measurements, Bretherton et al. (2004) showed an exponential  
93 relationship between rainfall and PWV over different tropical ocean areas. While the direction of  
94 causation in this relationship is not unambiguous *a priori*, this exponential relationship could be  
95 plausibly interpreted in terms of the moisture-convection feedbacks, in which the moister  
96 environment reduces the entrainment drying of updrafts and/or precipitation re-evaporation, and  
97 thus favors deep convection (Holloway & Neelin, 2009). The gradient of the precipitation-  
98 precipitable water curve has also been interpreted as the inverse of a moisture adjustment  
99 timescale (Bretherton et al., 2004; Adames, 2017). Based on GCM simulations, Hannah &  
100 Maloney (2011) found that both increasing the minimum entrainment parameter and increasing  
101 the rain evaporation fraction in the convective parameterization make the dependence of rainfall  
102 on column saturation fraction more nonlinear and more consistent with the observed relationship.  
103 These arguments taken together may be viewed as an empirical (and partial) support for the  
104 “moisture mode” framework. And within this framework, if the dependence of precipitation on  
105 PWV is weaker over the MC, e.g., due to a strong diurnal cycle, this weaker dependence may  
106 lead to a weaker “moisture mode” and contribute to the barrier effect.

107 It has been previously established with Tropical Rainfall Measuring Mission (TRMM)  
108 rainfall measurements that modulation of rainfall by the MJO is weaker over the MC compared  
109 to that over the surrounding oceans (Maloney & Sobel, 2004; Sakaeda et al., 2017). PWV over  
110 the MC is not available from the microwave measurements used in Bretherton et al. (2004)  
111 owing to the complications associated with land-surface emissivity. Roundy & Frank (2004)  
112 used data from the NASA Water Vapor Project (NVAP), but the data may be problematic over

113 the MC (Torri et al., 2019). Bergemann & Jakob (2016) used the ERA-Interim data from 1998 to  
114 2015 to study the rainfall-PWV relationship and found that coastally influence rainfall has a  
115 weaker dependence on mid-troposphere humidity than that over the open ocean. However, the  
116 accuracy of the ERA-Interim water vapor data over the Maritime Continent has not been well  
117 established, and over a substantial portion of the dataset time period, all-weather data such as  
118 that from GPS Radio Occultation was not available for assimilation. Torri et al. (2019) used data  
119 from the Sumatran GPS Array (SuGAR), a network of ground GPS stations in Sumatra  
120 established for geodesic studies (Feng et al., 2015), and found that the MJO modulates the  
121 diurnally averaged PWV over the archipelago and coastal stations by similar amounts (Fig. 12 in  
122 Torri et al. (2019)). If we take the coastal stations to be more land-like than the archipelago  
123 stations, these results imply a weaker dependence of rainfall on PWV over the different MJO  
124 phases over Sumatra.

125 In our work, we extend the work by Torri et al. (2019) in two ways. We first examine the  
126 dependence of rainfall on PWV more generally in a manner following the approach of  
127 Bretherton et al. (2004). Second, in addition to Sumatra, we extend the analysis to the entire MC  
128 region using ERA5 reanalysis data (Hersbach et al., 2020), which assimilates GPS radio  
129 occultation (RO) data. The GPS RO data show a good agreement with collocated ground-based  
130 GPS measurements in Torri et al. (2019)'s Fig.5. This work also revisits Bergemann & Jakob  
131 (2016) and Ahmed & Schumacher (2017) using the SuGAR dataset and the new ERA5 data. The  
132 comparison between reanalysis PWV and co-located SuGAR data (Figure 1bc) shows that ERA5  
133 has improved quality compared to ERA-Interim used in the previous work. Also, we divided the  
134 Maritime Continent into 4 geographic categories in order to investigate the change in rain-PWV  
135 relationship over different regions in more detail, while the MC is regarded as a whole in Ahmed  
136 & Schumacher (2017).

137 In section 2, we will introduce the datasets and methods. In subsections 3.1 and 3.2, we  
138 will present the results of the diurnal cycle of rainfall and PWV and relationship between rainfall  
139 and PWV. In subsection 3.3, we will investigate how the MJO modulates the PWV and rainfall  
140 over MC, and their linkage. In section 4, we will summarize the results and interpret the MC  
141 barrier effect using our findings.

## 142 **2 Data and Methods**

143 In this work, PWV is estimated using ground-based GPS-derived network data over  
144 Sumatra and ERA5 reanalysis over the Maritime Continent. We also use the Global precipitation  
145 measurement (GPM) rainfall data.

### 146 **2.1 PWV data from Sumatra GPS Array station (SuGAR)**

147 GPS relies on the transmission of radio wave signals from satellite to receiver in order to  
148 obtain precise positions. When these signals travel through the atmosphere, two potential sources  
149 of error arise due to refraction of the radio waves – the ionospheric delay, and the tropospheric  
150 delay. The delay due to the tropospheric component (tropospheric path delay) in the neutral  
151 atmosphere (troposphere and stratosphere) can be further divided into the hydrostatic delay and  
152 the wet delay, the latter of which, when mapped to the zenith angle, can be used to obtain  
153 precipitable water data (Askne & Nordius, 1987). The relative insensitivity of L-band radio  
154 signals to cloud and droplet makes the GPS-PWV product available in all weather conditions. In  
155 our study, as in Torri et al. (2019), we use data from 45 GPS stations over Sumatra during the

156 period of 2008-2013 (Feng et al., 2015). We divide the stations into three categories: the small  
157 islands west of Sumatra (ocean), the coast along Sumatra (coast), and inland (land) as shown in  
158 Fig. 1a.

## 159 2.2 PWV data over the MC from ERA5 reanalysis

160 As for the PWV data over the broader Maritime Continent (10°S-10°N, 90°E-150°E), we  
161 utilize ERA5, the latest global atmospheric reanalysis dataset released by the European Centre  
162 for Medium-range Weather Forecasts. The Constellation Observing System for Meteorology,  
163 Ionosphere, and Climate Version 1&2 (COSMIC1&2) radio occultation measurements, which  
164 can provide information on temperature and humidity based on the signal refraction, were  
165 assimilated into ERA5 since 2006 and 2020, respectively. The ERA5 reanalysis PWV data  
166 compare well with COSMIC1&2 over the Maritime Continent (Fig. S1) and provide a better  
167 temporal and spatial coverage. Therefore, we use ERA5 PWV data whose time resolution is 1  
168 hour, and spatial resolution is 0.25°, over the Maritime Continent during 2005-2016. Based on  
169 ERA5 land fraction data, we divide the Maritime Continent area into ocean (land fraction<0.1),  
170 coast (0.1<land fraction<0.8) and land (land fraction>0.8) grids, which is similar to the three  
171 categories of SuGAR stations. As PWV is the integral of column of water vapor above the  
172 ground, a higher elevation means a shorter integration path and a naturally lower PWV value.  
173 Therefore, we exclude grids where the elevation is higher than 150 meters from the three  
174 categories above and reclassify them as mountainous regions, so that regions remain classified as  
175 “land” and “coast” can better compare with the “ocean”.

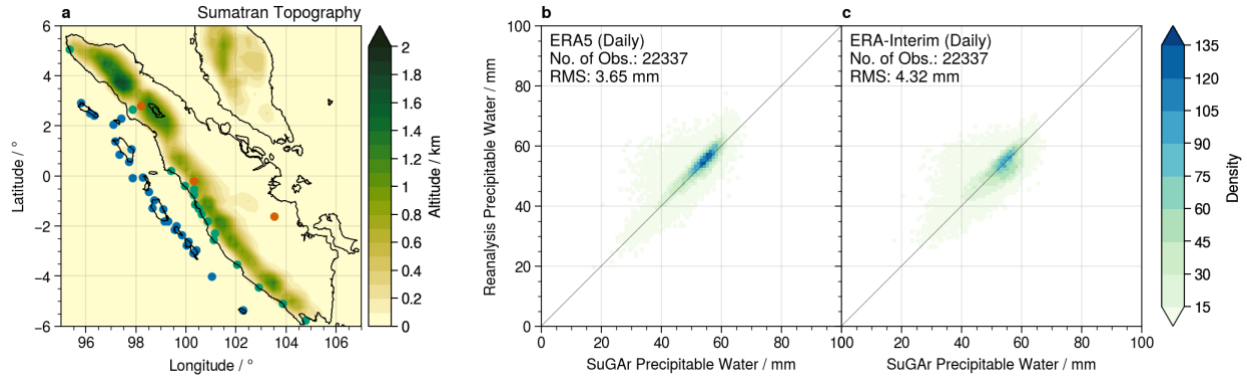
## 176 2.3 Rainfall data from Global Precipitation Measurement

177 The Global Precipitation Measurement (GPM) is the successor to TRMM. It has two  
178 advanced instruments, Dual-frequency Precipitation Radar and a radiometer called GPM  
179 Microwave Imager, which allows GPM to measure precipitation intensity and type through all  
180 cloud layers using a wider data swath (Skofronick-Jackson et al., 2018). The Integrated Multi-  
181 Satellite Retrievals for GPM (IMERGv6) we use here, is the Level 3 precipitation estimation  
182 product of GPM, which intercalibrate, merge, and interpolate satellite microwave precipitation  
183 estimates with microwave calibrated infrared (IR) satellite estimates, precipitation gauge  
184 analyses at high spatio-temporal resolution of 30 minutes and 0.1°. In order to do a comparison  
185 with the PWV data, we average the higher-resolution GPM 0.1° by 0.1° data to a coarser 0.25° by  
186 0.25° grid exported by the ERA5 reanalysis.

## 187 2.4 RMM MJO index

188 Wheeler and Hendon (2004) developed the Real-time Multivariate MJO (RMM) index to  
189 compute the state of the MJO using latitudinal averages of outgoing longwave radiation and  
190 zonal wind at 200 and 850 hPa in the tropics. This index has become the standard method used to  
191 describe the approximate center and phase of the MJO as it propagates along the equator. Based  
192 on the rainfall (Fig. S6), we assign RMM MJO phases 2, 3, 4, 5 as active MJO phases and phases  
193 1, 6, 7, 8 as suppressed phases over the MC.

194



195

196 **Figure 1.** (a) The GPS stations are divided into three categories: ocean (blue), coast (green), land  
 197 (red). The shading shows the orography. The comparison of PWV (b) between ERA5 and SuGAR  
 198 and (c) between ERA-Interim and SuGAR.

### 199 3 Results

#### 200 3.1 Modulations of the diurnal cycle of PWV and rainfall by the MJO

201 Previous studies suggest that the diurnal cycle of precipitation and related sub-MJO-scale  
 202 features compete with the MJO for moist static energy, which may explain the MC barrier effect  
 203 (Neale & Slingo, 2003; Sakaeda et al., 2017; Ling et al., 2019). Here we extend the diurnal cycle  
 204 of PWV over Sumatra investigated by Torri et al. (2019) to the whole Maritime Continent and  
 205 also include the diurnal cycle of rainfall at different MJO phases. First we examine the diurnal  
 206 cycle of PWV over Sumatra with more coastal ground-based GPS stations compared to Fujita et  
 207 al. (2011). Figure S2 indicates that the diurnal cycle of PWV in this work has a clear sinusoidal  
 208 pattern, with a peak at about 19:00 local time, which is different from the midnight peak time  
 209 over the coastal stations in Fujita et al. (2011). With 6 years of data, the diurnal cycle of PWV  
 210 over Sumatra in our Figure S3 compares well with Torri et al. (2019)'s Fig. 11, which used 6  
 211 months of data to show that when the MJO transitions from suppressed to active phases, PWV  
 212 increases by roughly the same amount throughout the day across all surface types. The  
 213 modulation of the rainfall diurnal cycle by the MJO is substantial over both land and ocean, but  
 214 is stronger over the ocean than over the land (Figure S4). The diurnal cycles of rainfall and PWV  
 215 over the whole Maritime Continent (Fig. S5&S6) show a similar behavior.

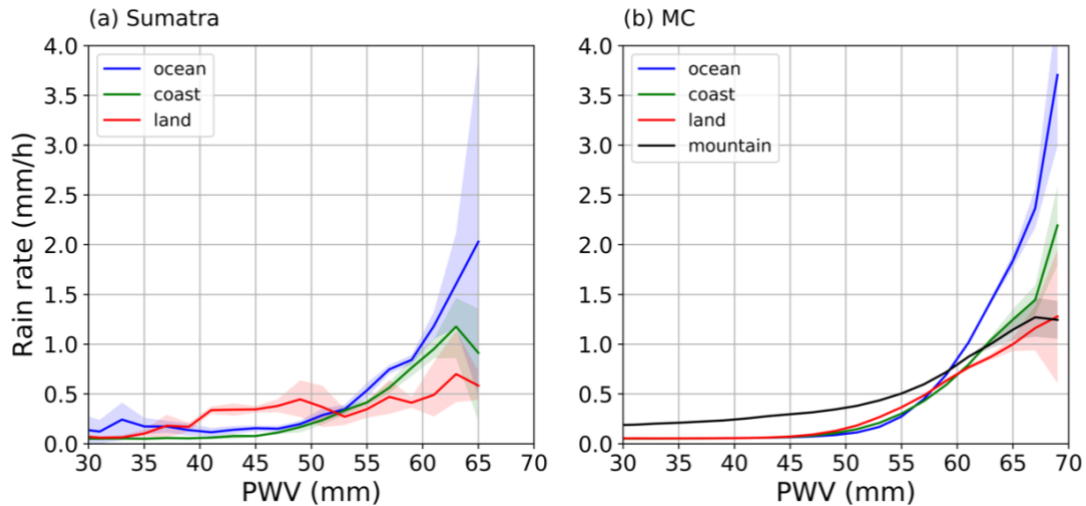
#### 216 3.2 Relationship between daily PWV and precipitation over the Maritime Continent

217 In this section, we examine the relationship between the daily averaged PWV and  
 218 precipitation over land and ocean.

219 We first examine this relationship using Sumatra GPS data (Figure 2a). Across all surface  
 220 types (ocean, coast and land), the precipitation rate is on average below 0.5 mm/h when PWV is  
 221 below 55 mm. Over ocean, the rain-PWV relationship curve sharply increases when PWV is  
 222 above 55 mm, which is similar to what Bretherton et al. (2004) found over tropical oceans. At  
 223 the same time, when PWV is higher than 55 mm the precipitation rate over land is lower than  
 224 over the coast and much lower than over the ocean. The next question is, is Sumatra  
 225 representative of the broader MC area?

226 Figure 2b shows the relationship between PWV and rainfall over the MC using 12 years  
 227 of ERA5 PWV data and GPM IMERG precipitation data. Precipitation rate over the ocean

228 increases exponentially when PWV is above 55 mm, approaches 2 mm/h when PWV reaches 65  
 229 mm, which is similar to the results over Sumatra (Figure 2a). In contrast, the rain-PWV curves  
 230 over land and coast are less steep than that over ocean. At similar PWV values, the precipitation  
 231 rate over land is lower than over the ocean, which confirms a weaker rain dependence on PWV  
 232 over the Maritime Continent.



233

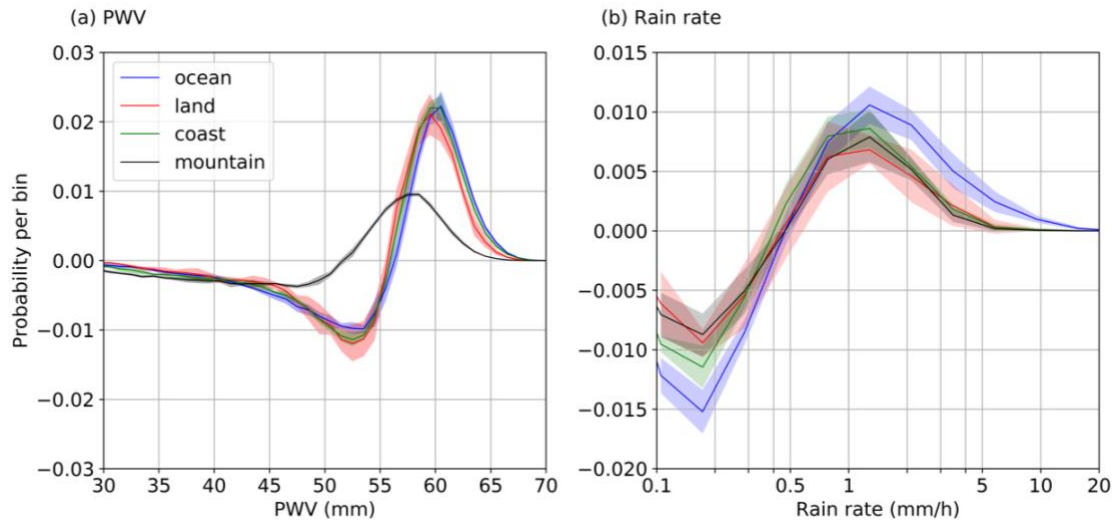
234 **Figure 2.** Relationship between daily rainfall and daily precipitable water vapor over (a) Sumatra  
 235 and (b) the Maritime Continent, for oceanic areas (blue), coastal areas (green), land areas (red)  
 236 and mountain areas (black). The shadings show the 95% confidence interval of the mean,  
 237 estimated by using t-test and dividing the data into 5 groups. Data are not shown above 65 mm  
 238 for Sumatra (69 mm for the MC) due to limited occurrences of such high PWV values.

### 239 3.3 PWV and rainfall modulation by the MJO

240 Figure 3a shows the difference in the probability distribution functions (PDF) of daily-  
 241 aggregated PWV between MJO active phases (Fig. S7a) and suppressed phases (Fig. S7b) over  
 242 the Maritime continent. The difference in probability distribution of PWV shows a dipole  
 243 pattern, corresponding to the PWV values shift between the different MJO phases. Except for the  
 244 mountain grids, frequencies of PWV below (above) 57 mm decreased (increased), with a peak  
 245 frequency decrease (increase) at 53mm (61 mm) with enhanced MJO convection. Note that this  
 246 shift is remarkably similar over ocean, coast and land, except over mountainous regions, where  
 247 the spectrum shifts to lower PWV values. Therefore the PWV modulation by the MJO is no  
 248 weaker over the MC land compared to over the ocean.

249 Figure 3b shows the difference in the distributions of log precipitation rates between the  
 250 active and suppressed MJO phases. This difference between the active phase and suppressed  
 251 phase, is positive (negative) when precipitation rate is higher (lower) than about 0.5 mm/hr over  
 252 all regions, corresponding to the strong convection during the active phase of the MJO over the  
 253 MC. In contrast, the change in rainfall rate is larger over the ocean than over both land and  
 254 coastal regions, which means the MJO modulation of precipitation rate is stronger over the  
 255 surrounding ocean area than the MC. The frequency of high rainfall rates greater than 1 mm/hr is  
 256 larger over ocean than land during the active MJO phases.

257 To summarize, the MJO has similar influences on PWV for different surface types, but  
 258 has a weaker effect on the precipitation rate over land as compared to over the surrounding ocean  
 259 area. This contrast between land and ocean, which is consistent with the weaker convection  
 260 modulation over land found by Zhang & Ling (2017) and others, may be interpreted in terms of  
 261 the difference in the sensitivity of rainfall on PWV between land and ocean.



262

263 **Figure 3.** Difference of the distributions of (a) precipitable water vapor and (b) log rainfall rate  
 264 during the MJO active phases relative to the suppressed phases for ocean grids (blue), coast grids  
 265 (green), land grids (red) and mountain grids (black) over the MC. Bin size is 1mm for PWV and  
 266 0.217 in  $\log_{10}$ (precipitation rate) scale, respectively. The shadings show the 95% confidence  
 267 interval of the mean, estimated by using t-test and dividing the data into 5 groups.

#### 268 4. Summary and discussion

269 This work is inspired by the “moisture mode” framework, in which a prognostic column  
 270 moisture equation is the key to the MJO dynamics. One of the supporting evidence of the  
 271 “moisture mode” theory is the observed exponential rain-PWV relationship over the tropical  
 272 oceans (Bretherton et al., 2004), which shows that precipitation is highly sensitive to column  
 273 water vapor (or column relative humidity). In this work, we utilized the PWV derived from  
 274 ground-based GPS stations over Sumatra, which are relatively unaffected by cloudy and rainy  
 275 conditions or land-surface emissivity, and extend the study to the whole MC with ERA5, which  
 276 assimilates GPS radio occultation data and shows good agreement with SuGAR.

277 We find a clear rain-PWV relationship over all surface types (i.e., ocean, land, and coast  
 278 areas), which is consistent with previous studies. However, the dependence of rainfall on PWV is  
 279 weaker over land and coast than over ocean. We also find that the MJO enhances the PWV by  
 280 roughly similar amounts over land and ocean, and suggest that the weaker modulation of rainfall  
 281 rate by the MJO over land compared to that over ocean may be a consequence of its weaker  
 282 dependence of rainfall on PWV. This in turn may lead to a weaker “moisture mode” that  
 283 partially explains the MC’s barrier effect on the MJO. Whether and how a weaker rain-PWV  
 284 dependence over land is related to its stronger diurnal cycle will be further investigated through  
 285 numerical simulations in the future.

286 The rain-PWV dependence is only one aspect of the MJO dynamics within the moisture  
287 mode framework. While our results suggest the weaker rain-PWV dependence over land as a  
288 potential factor for the general weakening of the MJO over the MC, other reasons as to why  
289 some MJO events stall and some propagate through the MC could be differences in the mean  
290 state, or just generally the diversity of MJO events as recently highlighted by Wang et al. (2019).  
291 Zhang & Ling (2017) found that the land-to-ocean precipitation ratio is higher for the non-MC  
292 crossing events and proposed that the competition between land and oceanic convection is key to  
293 the varying strengths of the barrier effect. Ahn et al. (2020) produced this association in GCMs,  
294 provided the interpretation that the weaker MC land convection results in steepening of the  
295 vertical and meridional mean moisture gradient over the MC, and the MSE advection further  
296 enhances the MJO eastward propagation. It is however also possible that a higher land-to-ocean  
297 rain ratio gives land convection, and its weaker PWV dependence, a greater role in the MJO  
298 dynamics, consistent with our hypothesis. Many other aspects can affect the MJO propagation  
299 through the MC as well. For example, Kim et al. (2014) suggested that whether MJO convection  
300 over the Indian Ocean can cross over the MC is closely associated with the dry anomalies over  
301 the eastern MC and west Pacific. The positive moisture meridional advection by the anomalous  
302 poleward flow, which is interpreted as part of the Rossby wave response to the dry anomaly,  
303 moistens the atmosphere to the east of MJO convection, which helps MJO eastward propagation.  
304 More generally, the horizontal moisture advection by MJO anomalous wind acting upon the  
305 mean state moisture gradient is argued as key to the MJO propagation, with the MJO detouring  
306 to the south of the MC during the boreal winter as a good example (Jiang, 2017; Kim et al.,  
307 2017). Our suggestion is compatible with these arguments within the moisture mode framework,  
308 as various processes modify the column moisture, leading to the strengthening/weakening or  
309 propagation of the column moisture anomaly.

310 Many recent modeling studies suggest that the moisture–convection feedbacks and the  
311 MJO variability can be strengthened in GCMs by increasing the sensitivity of the convective  
312 scheme to free tropospheric moisture (Waliser et al., 2009; Zhu et al., 2009; Kim & Kang, 2012),  
313 e.g., with the use of a specified convective rain evaporation fraction (Grabowski & Moncrieff,  
314 2004). That modern models tend to exaggerate the barrier effect could therefore be due to poor  
315 representations of the mean state moisture (Gonzalez & Jiang, 2017), or overly strong MC land  
316 convection (Ahn et al., 2020). Our results suggest that the rain-PWV dependences over land and  
317 ocean in the GCMs could be another valuable diagnosis.

## 318 **Acknowledgments and Data**

319 The study was supported by NOAA Climate Program Office grant  
320 NA17OAR4310260. The authors thank two anonymous reviewers for their constructive reviews.  
321 Siyue Chen acknowledges Hongqing Wang for his support and some insightful comments on this  
322 work. We are grateful to Dr. Emma Hill, the Earth Observatory of Singapore at Nanyang  
323 Technological University and the Indonesian Institute of Science (LIPI) for operating the SuGAR  
324 network and sharing the ground GPS data. We acknowledge David K. Adams and Giuseppe  
325 Torri for producing and deriving SuGAR PWV data. We also acknowledge the NASA, NOAA  
326 and ECMWF for producing and making available the data used in this study and the Harvard  
327 FAS Science Division Research Computing Group for computing support. The SuGAR PWV  
328 data is available on <https://doi.org/10.7910/DVN/J1MKHJ>. The ERA5 data is from  
329 <https://www.ecmwf.int/en/forecasts/datasets/reanalysis-datasets/era5>, the GPM data is from

330 <https://gpm.nasa.gov/taxonomy/term/1417>, and the RMM MJO index is from  
 331 <https://psl.noaa.gov/mjo/mjoindex/>.

332

### 333 **References:**

- 334 Adames, Á. F. (2017). Precipitation budget of the Madden-Julian oscillation. *Journal of the*  
 335 *Atmospheric Sciences*, 74(6), 1799–1817. <https://doi.org/10.1175/JAS-D-16-0242.1>
- 336 Adames, Á. F., & Kim, D. (2016). The MJO as a dispersive, convectively coupled moisture  
 337 wave: Theory and observations. *Journal of the Atmospheric Sciences*, 73(3), 913–941.  
 338 <https://doi.org/10.1175/JAS-D-15-0170.1>
- 339 Adames, Á. F., & Maloney, E. D. (2021). Moisture Mode Theory’s Contribution to Advances in  
 340 our Understanding of the Madden-Julian Oscillation and Other Tropical Disturbances.  
 341 *Current Climate Change Reports*, 7(2), 72–85. <https://doi.org/10.1007/s40641-021-00172-4>
- 342 Ahmed, F., & Schumacher, C. (2017). Geographical differences in the tropical precipitation-  
 343 moisture relationship and rain intensity onset. *Geophysical Research Letters*, 44(2), 1114–  
 344 1122. <https://doi.org/10.1002/2016GL071980>
- 345 Ahn, M. S., Kim, D., Ham, Y. G., & Park, S. (2020). Role of maritime continent land convection  
 346 on the mean state and MJO propagation. *Journal of Climate*, 33(5), 1659–1675.  
 347 <https://doi.org/10.1175/JCLI-D-19-0342.1>
- 348 Andersen, J. A., & Kuang, Z. (2012). Moist static energy budget of MJO-like disturbances in the  
 349 atmosphere of a zonally symmetric aquaplanet. *Journal of Climate*, 25(8), 2782–2804.  
 350 <https://doi.org/10.1175/JCLI-D-11-00168.1>
- 351 Arcodia, M. C., Kirtman, B. P., & Siqueira, L. S. P. (2020). How MJO Teleconnections and  
 352 ENSO Interference Impacts U.S. Precipitation. *Journal of Climate*, 33(11), 4621–4640.  
 353 <https://doi.org/10.1175/JCLI-D-19-0448.1>
- 354 Askne, J., & Nordius, H. (1987). Estimation of tropospheric delay for microwaves from surface  
 355 weather data. *Radio Science*, 22(03), 379–386. <https://doi.org/10.1029/RS022i003p00379>
- 356 Barrett, B. S. (2019). Connections between the Madden–Julian Oscillation and surface  
 357 temperatures in winter 2018 over eastern North America. *Atmospheric Science Letters*,  
 358 20(1), 1–8. <https://doi.org/10.1002/asl.869>
- 359 Bergemann, M., & Jakob, C. (2016). How important is tropospheric humidity for coastal rainfall  
 360 in the tropics ?, (May). <https://doi.org/10.1002/2016GL069255.1>.
- 361 Bretherton, C. S., Peters, M. E., & Back, L. E. (2004). Relationships between water vapor path  
 362 and precipitation over the tropical oceans. *Journal of Climate*, 17(7), 1517–1528.  
 363 [https://doi.org/10.1175/1520-0442\(2004\)017<1517:RBWVPA>2.0.CO;2](https://doi.org/10.1175/1520-0442(2004)017<1517:RBWVPA>2.0.CO;2)
- 364 Feng, L., Hill, E. M., Banerjee, P., Hermawan, I., Tsang, L. L. H., Natawidjaja, D. H., et al.  
 365 (2015). A unified GPS-based earthquake catalog for the Sumatran plate boundary between  
 366 2002 and 2013. *Journal of Geophysical Research: Solid Earth*, 120(5), 3566–3598.  
 367 <https://doi.org/10.1002/2014JB011661>
- 368 Fujita, M., Yoneyama, K., Mori, S., Nasuno, T., & Satoh, M. (2011). Diurnal convection peaks  
 369 over the eastern Indian Ocean off sumatra during different MJO phases. *Journal of the*

- 370 *Meteorological Society of Japan*, 89(A), 317–330. <https://doi.org/10.2151/jmsj.2011-A22>
- 371 Gonzalez, A. O., & Jiang, X. (2017). Winter mean lower tropospheric moisture over the  
372 Maritime Continent as a climate model diagnostic metric for the propagation of the  
373 Madden-Julian oscillation. *Geophysical Research Letters*, 44(5), 2588–2596.  
374 <https://doi.org/10.1002/2016GL072430>
- 375 Grabowski, W. W., & Moncrieff, M. W. (2004). Moisture-convection feedback in the tropics.  
376 *Quarterly Journal of the Royal Meteorological Society*, 130 C(604), 3081–3104.  
377 <https://doi.org/10.1256/qj.03.135>
- 378 Hagos, S. M., Zhang, C., Feng, Z., Burleyson, C. D., De Mott, C., Kerns, B., et al. (2016). The  
379 impact of the diurnal cycle on the propagation of Madden-Julian Oscillation convection  
380 across the Maritime Continent. *Journal of Advances in Modeling Earth Systems*, 8(4),  
381 1552–1564. <https://doi.org/10.1002/2016MS000725>
- 382 Hannah, W. M., & Maloney, E. D. (2011). The role of moisture-convection feedbacks in  
383 simulating the Madden-Julian oscillation. *Journal of Climate*, 24(11), 2754–2770.  
384 <https://doi.org/10.1175/2011JCLI3803.1>
- 385 Hersbach, H., Bell, B., Berrisford, P., Hirahara, S., Horányi, A., Muñoz-Sabater, J., et al. (2020).  
386 The ERA5 global reanalysis. *Quarterly Journal of the Royal Meteorological Society*,  
387 146(730), 1999–2049. <https://doi.org/10.1002/qj.3803>
- 388 Holloway, C. E., & Neelin, D. J. (2009). Moisture vertical structure, column water vapor, and  
389 tropical deep convection. *Journal of the Atmospheric Sciences*, 66(6), 1665–1683.  
390 <https://doi.org/10.1175/2008JAS2806.1>
- 391 Inness, P. M., & Slingo, J. M. (2006). The interaction of the Madden-Julian Oscillation with the  
392 Maritime Continent in a GCM. *Quarterly Journal of the Royal Meteorological Society*,  
393 132(618 A), 1645–1667. <https://doi.org/10.1256/qj.05.102>
- 394 Inness, P. M., Slingo, J. M., Guilyardi, E., & Cole, J. (2003). Simulation of the Madden-Julian  
395 oscillation in a coupled general circulation model. Part II: The role of the basic state.  
396 *Journal of Climate*, 16(3), 365–382. [https://doi.org/10.1175/1520-  
397 0442\(2003\)016<0365:SOTMJO>2.0.CO;2](https://doi.org/10.1175/1520-0442(2003)016<0365:SOTMJO>2.0.CO;2)
- 398 Jiang, X. (2017). Key processes for the eastward propagation of the madden-julian oscillation  
399 based on multimodel simulations. *Journal of Geophysical Research*, 122(2), 755–770.  
400 <https://doi.org/10.1002/2016JD025955>
- 401 Kiladis, G. N., & Weickmann, K. M. (1992). Circulation Anomalies Associated with Tropical  
402 Convection during Northern Winter. *Monthly Weather Review*, 120(9), 1900–1923.  
403 [https://doi.org/10.1175/1520-0493\(1992\)120<1900:CAAWTC>2.0.CO;2](https://doi.org/10.1175/1520-0493(1992)120<1900:CAAWTC>2.0.CO;2)
- 404 Kim, D., & Kang, I. S. (2012). A bulk mass flux convection scheme for climate model:  
405 Description and moisture sensitivity. *Climate Dynamics*, 38(1–2), 411–429.  
406 <https://doi.org/10.1007/s00382-010-0972-2>
- 407 Kim, D., Kug, J. S., & Sobel, A. H. (2014). Propagating versus nonpropagating Madden-Julian  
408 oscillation events. *Journal of Climate*, 27(1), 111–125. [https://doi.org/10.1175/JCLI-D-13-  
409 00084.1](https://doi.org/10.1175/JCLI-D-13-00084.1)
- 410 Kim, D., Kim, H., & Lee, M. I. (2017). Why does the MJO detour the Maritime Continent during

- 411 austral summer? *Geophysical Research Letters*, 44(5), 2579–2587.  
 412 <https://doi.org/10.1002/2017GL072643>
- 413 Ling, J., Zhang, C., Joyce, R., Xie, P. ping, & Chen, G. (2019). Possible Role of the Diurnal  
 414 Cycle in Land Convection in the Barrier Effect on the MJO by the Maritime Continent.  
 415 *Geophysical Research Letters*, 46(5), 3001–3011. <https://doi.org/10.1029/2019GL081962>
- 416 Madden, R. A., & Julian, P. R. (1971). Detection of a 40–50 Day Oscillation in the Zonal Wind  
 417 in the Tropical Pacific. *Journal of the Atmospheric Sciences*, 28(5), 702–708.  
 418 [https://doi.org/10.1175/1520-0469\(1971\)028<0702:doadoi>2.0.co;2](https://doi.org/10.1175/1520-0469(1971)028<0702:doadoi>2.0.co;2)
- 419 Madden, R. A., & Julian, P. R. (1972). Description of Global-Scale Circulation Cells in the  
 420 Tropics with a 40–50 Day Period. *Journal of the Atmospheric Sciences*, 29(6), 1109–1123.  
 421 [https://doi.org/10.1175/1520-0469\(1972\)029<1109:DOGSCC>2.0.CO;2](https://doi.org/10.1175/1520-0469(1972)029<1109:DOGSCC>2.0.CO;2)
- 422 Majda, A. J., & Yang, Q. (2016). A multiscale model for the intraseasonal impact of the diurnal  
 423 cycle over the maritime continent on the Madden-Julian oscillation. *Journal of the*  
 424 *Atmospheric Sciences*, 73(2), 579–604. <https://doi.org/10.1175/JAS-D-15-0158.1>
- 425 Maloney, E. D., & Sobel, A. H. (2004). Surface fluxes and ocean coupling in the tropical  
 426 intraseasonal oscillation. *Journal of Climate*, 17(22), 4368–4386.  
 427 <https://doi.org/10.1175/JCLI-3212.1>
- 428 Mo, K. C. (2000). Intraseasonal modulation of summer precipitation over North America.  
 429 *Monthly Weather Review*, 128(5), 1490–1505. [https://doi.org/10.1175/1520-0493\(2000\)128<1490:IMOSPO>2.0.CO;2](https://doi.org/10.1175/1520-0493(2000)128<1490:IMOSPO>2.0.CO;2)
- 431 Neale, R., & Slingo, J. (2003). The Maritime Continent and its role in the global climate: A  
 432 GCM study. *Journal of Climate*, 16(5), 834–848. [https://doi.org/10.1175/1520-0442\(2003\)016<0834:TMCAIR>2.0.CO;2](https://doi.org/10.1175/1520-0442(2003)016<0834:TMCAIR>2.0.CO;2)
- 434 Rauniyar, S. P., & Walsh, K. J. E. (2011). Scale interaction of the diurnal cycle of rainfall over  
 435 the Maritime Continent and Australia: Influence of the MJO. *Journal of Climate*, 24(2),  
 436 325–348. <https://doi.org/10.1175/2010JCLI3673.1>
- 437 Raymond, D. J. (2001). A New Model of the Madden-Julian Oscillation. *Journal of the*  
 438 *Atmospheric Sciences*, 58(18), 2807–2819. [https://doi.org/10.1175/1520-0469\(2001\)058<2807:ANMOTM>2.0.CO;2](https://doi.org/10.1175/1520-0469(2001)058<2807:ANMOTM>2.0.CO;2)
- 440 Roundy, P. E., & Frank, W. M. (2004). Effects of low-frequency wave interactions on  
 441 intraseasonal oscillations. *Journal of the Atmospheric Sciences*, 61(24), 3025–3041.  
 442 <https://doi.org/10.1175/JAS-3348.1>
- 443 Rui, H., & Wang, B. (1990). Development Characteristics and Dynamic Structure of Tropical  
 444 Intraseasonal Convection Anomalies. *Journal of the Atmospheric Sciences*.  
 445 [https://doi.org/10.1175/1520-0469\(1990\)047<0357:dcadso>2.0.co;2](https://doi.org/10.1175/1520-0469(1990)047<0357:dcadso>2.0.co;2)
- 446 Sakaeda, N., Kiladis, G., & Dias, J. (2017). The diurnal cycle of tropical cloudiness and rainfall  
 447 associated with the Madden-Julian oscillation. *Journal of Climate*, 30(11), 3999–4020.  
 448 <https://doi.org/10.1175/JCLI-D-16-0788.1>
- 449 Schreck, C. J., Cordeira, J. M., & Margolin, D. (2013). Which MJO events affect north american  
 450 temperatures? *Monthly Weather Review*, 141(11), 3840–3850.  
 451 <https://doi.org/10.1175/MWR-D-13-00118.1>

- 452 Seo, K. H., Wang, W., Gottschalck, J., Zhang, Q., Schemm, J. K. E., Higgins, W. R., & Kumar,  
453 A. (2009). Evaluation of MJO forecast skill from several statistical and dynamical forecast  
454 models. *Journal of Climate*, 22(9), 2372–2388. <https://doi.org/10.1175/2008JCLI2421.1>
- 455 Skofronick-Jackson, G., Kirschbaum, D., Petersen, W., Huffman, G., Kidd, C., Stocker, E., &  
456 Kakar, R. (2018). The Global Precipitation Measurement (GPM) mission’s scientific  
457 achievements and societal contributions: reviewing four years of advanced rain and snow  
458 observations. *Quarterly Journal of the Royal Meteorological Society*, 144(April), 27–48.  
459 <https://doi.org/10.1002/qj.3313>
- 460 Sobel, A., & Maloney, E. (2012). An idealized semi-empirical framework for modeling the  
461 Madden-Julian oscillation. *Journal of the Atmospheric Sciences*, 69(5), 1691–1705.  
462 <https://doi.org/10.1175/JAS-D-11-0118.1>
- 463 Sobel, A., & Maloney, E. (2013). Moisture modes and the eastward propagation of the MJO.  
464 *Journal of the Atmospheric Sciences*, 70(1), 187–192. <https://doi.org/10.1175/JAS-D-12-0189.1>
- 466 Tian, B., Waliser, D. E., & Fetzer, E. J. (2006). Modulation of the diurnal cycle of tropical deep  
467 convective clouds by the MJO. *Geophysical Research Letters*, 33(20), 1–6.  
468 <https://doi.org/10.1029/2006GL027752>
- 469 Tippett, M. K. (2018). Robustness of relations between the MJO and U.S. tornado occurrence.  
470 *Monthly Weather Review*, 146(11), 3873–3884. <https://doi.org/10.1175/MWR-D-18-0207.1>
- 471 Torri, G., Adams, D. K., Wang, H., & Kuang, Z. (2019). On the diurnal cycle of GPS-derived  
472 precipitable water vapor over sumatra. *Journal of the Atmospheric Sciences*, 76(11), 3529–  
473 3552. <https://doi.org/10.1175/JAS-D-19-0094.1>
- 474 Vitart, F., & Molteni, F. (2010). Simulation of the Madden-Julian oscillation and its  
475 teleconnections in the ECMWF forecast system. *Quarterly Journal of the Royal  
476 Meteorological Society*, 136(649), 842–855. <https://doi.org/10.1002/qj.623>
- 477 Waliser, D., Sperber, K., Hendon, H., Kim, D., Maloney, E., Wheeler, M., et al. (2009). MJO  
478 simulation diagnostics. *Journal of Climate*, 22(11), 3006–3030.  
479 <https://doi.org/10.1175/2008JCLI2731.1>
- 480 Wang, B., Chen, G., & Liu, F. (2019). Diversity of the Madden-Julian Oscillation. *Science  
481 Advances*, 5(7), eaax0220. <https://doi.org/10.1126/sciadv.aax0220>
- 482 Wang, S., Sobel, A. H., Tippett, M. K., & Vitart, F. (2019). Prediction and predictability of  
483 tropical intraseasonal convection: seasonal dependence and the Maritime Continent  
484 prediction barrier. *Climate Dynamics*, 52(9–10), 6015–6031.  
485 <https://doi.org/10.1007/s00382-018-4492-9>
- 486 Weaver, S. J., Wang, W., Chen, M., & Kumar, A. (2011). Representation of MJO Variability in  
487 the NCEP Climate Forecast System. *Journal of Climate*, 24(17), 4676–4694.  
488 <https://doi.org/10.1175/2011JCLI4188.1>
- 489 Wheeler, M. C., & Hendon, H. H. (2004). An all-season real-time multivariate MJO index:  
490 Development of an index for monitoring and prediction. *Monthly Weather Review*, 132(8),  
491 1917–1932. [https://doi.org/10.1175/1520-0493\(2004\)132<1917:AARMMI>2.0.CO;2](https://doi.org/10.1175/1520-0493(2004)132<1917:AARMMI>2.0.CO;2)
- 492 Wu, C. H., & Hsu, H. H. (2009). Topographic influence on the MJO in the maritime continent.

- 493 *Journal of Climate*, 22(20), 5433–5448. <https://doi.org/10.1175/2009JCLI2825.1>
- 494 Yamanaka, M. D. (2016). Physical climatology of Indonesian maritime continent: An outline to  
495 comprehend observational studies. *Atmospheric Research*, 178–179, 231–259.  
496 <https://doi.org/10.1016/j.atmosres.2016.03.017>
- 497 Zhang, C. (2005). Madden-Julian Oscillation. *Rev. Geophys*, (43), RG2003.  
498 <https://doi.org/10.1029/2004RG000158>
- 499 Zhang, C., & Ling, J. (2017). Barrier effect of the Indo-Pacific Maritime Continent on the MJO:  
500 Perspectives from tracking MJO precipitation. *Journal of Climate*, 30(9), 3439–3459.  
501 <https://doi.org/10.1175/JCLI-D-16-0614.1>
- 502 Zhou, Y., Lu, Y., Yang, B., Jiang, J., Huang, A., Zhao, Y., et al. (2016). On the relationship  
503 between the Madden-Julian Oscillation and 2m air temperature over central Asia in boreal  
504 winter. *Journal of Geophysical Research*, 121(22), 13,250–13,272.  
505 <https://doi.org/10.1002/2016JD025651>
- 506 Zhu, H., Hendon, H., & Jakob, C. (2009). Convection in a parameterized and superparameterized  
507 model and its role in the representation of the MJO. *Journal of the Atmospheric Sciences*,  
508 66(9), 2796–2811. <https://doi.org/10.1175/2009JAS3097.1>
- 509